Petroleum Science 21 (2024) 445–457

Contents lists available at ScienceDirect

Petroleum Science

journal homepage: www.keaipublishing.com/en/journals/petroleum-science

Original Paper

Impacts of proppant distribution on development of tight oil reservoirs with threshold pressure gradient

Ming Yue [a, b], Wei-Yao Zhu [b, **], Fei-Fei Gou [a], Tian-Ru Song [b], Yu-Chun You [a], Qi-Tao Zhang [b, *]

[a] State Key Laboratory of Shale Oil and Gas Enrichment Mechanisms and Effective Development, Beijing, 102206, China
[b] School of Civil and Resource Engineering, University of Science and Technology Beijing, Beijing, 100083, China

ARTICLE INFO

Article history:
Received 5 January 2023
Received in revised form
25 August 2023
Accepted 26 August 2023
Available online 26 August 2023

Edited by Yan-Hua Sun

Keywords:
Proppant distribution
Tight oil reservoir
Multi-stage fractured horizontal well
Threshold pressure gradient
Moving boundary

ABSTRACT

Field evidence indicates that proppant distribution and threshold pressure gradient have great impacts on well productivity. Aiming at the development of unconventional oil reservoirs in Triassic Chang-7 Unit, Ordos Basin of China, we presented an integrated workflow to investigate how (1) proppant placement in induced fracture and (2) non-linear flow in reservoir matrix would affect well productivity and fluid flow in the reservoir. Compared with our research before (Yue et al., 2020), here we extended this study into the development of multi-stage fractured horizontal wells (MFHWs) with large-scale complicated fracture geometry. The integrated workflow is based on the finite element method and consists of simulation models for proppant-laden fluid flow, fracture flow, and non-linear seepage flow, respectively. Simulation results indicate that the distribution of proppant inside the induced cracks significantly affects the productivity of the MFHW. When we assign an idealized proppant distribution instead of the real distribution, there will be an overestimation of 44.98% in daily oil rate and 30.63% in cumulative oil production after continuous development of 1000 days. Besides, threshold pressure gradient (TPG) also significantly affects the well performance in tight oil reservoirs. If we simply apply linear Darcy's law to the reservoir matrix, the overall cumulative oil production can be overrated by 77% after 1000 days of development. In general, this research provides new insights into the development of tight oil reservoirs with TPG and meanwhile reveals the significance of proppant distribution and non-linear fluid flow in the production scenario design.

1. Introduction

Nowadays, tight oil is considered as one of the most significant unconventional resources to meet the energy demand of China (Guo et al., 2019). During the development of unconventional oil resources in the Chang-7 Unit, two factors should be especially honored, which are (1) proppant distribution in the induced fractures (Hu et al., 2018), and (2) non-linear fluid flow in the reservoir matrix (Liu, 2019; Zeng et al., 2010, 2011). In this research, we aim to study how proppant distribution and non-linear fluid flow would affect the exploitation of tight oil reservoirs, and how much productivity overestimation would be yielded if we neglect their impacts.

First, regarding the study of how proppants will be placed in induced fractures and how these proppant distributions will affect the production, many researchers conducted experimental and numerical research correspondingly in the past few years. Regarding the experimental studies, a visual proppant placement device was widely adopted for the identification of the shape of the proppant dune in the fractures during and after the sand injection process (Cleary and Fonseca Jr, 1992). By adopting such an experimental apparatus, researchers can clearly observe the sand settlement between "rigid" boards, and thus we can physically study the sand placement process in a narrow space, i.e., crack (Yao et al., 2022). According to different research objectives, this research can be fabricated with different geometry to physically simulate sand settling in fractures with different shapes or geometries.

* Corresponding author.
** Corresponding author.
E-mail addresses: zhuweiyao@ustb.edu.cn (W.-Y. Zhu), romainzhang1128@gmail.com (Q.-T. Zhang).

https://doi.org/10.1016/j.petsci.2023.08.030

However, this device may also have some limitations. First, the scale of real fractures should be much larger than that in the laboratory (Osiptsov, 2017) and additional dimensional analysis should be introduced into the research to make the experimental results convincing and reflect the real rule of sand placement in fractures. Besides, the roughness of real fracture faces should be distinctive from that in the laboratory (Suri et al., 2020) so more effort should be made in the model validation process. Finally, the results from the proppant placement experiments are difficult to be directly used for reservoir simulation and evaluation of well performance. Regarding the numerical studies, different numerical models and frameworks are proposed for distinctive research objectives. Based on a Lagrangian approach, Dontsov and Peirce (2014, 2015a, 2015b) study the sand placement inside the induced crack considering the fracture tip screen-out. Besides, on the basis of a two-fluid model, some researchers (Boronin and Osiptsov, 2010, 2014; Boronin et al., 2015; Osiptsov et al., 2016) presented an art-to-state simulator to study different proppant placement topics. Furthermore, Zhang et al. (2020) studied the effect of sand placement on vertical well development considering the existence of natural fractures. They found that, the neglect of unbalanced sand placement can bring an overrate for up to 38.4% in cumulative oil production after 900 days of a vertical well. Zhang and Dahi Taleghani (2022) studied the impact of sand placement in a tree-shaped fracture network on post-fracturing flowback behavior. In their model, geomechanics and proppant stress are especially focused on. Yu et al. (2015) studied how the unbalanced sand distribution can have an influence on the MFHW in shale gas reservoirs. However, in this study, the fractures for each stage are assumed to have the same length and fracture spacing, which is not realistic in the real field trial. More detailly, Wang and Elsworth (2018) studied how proppant distribution will impact the variation process of the conductivity of the induced cracks. Their results show that, regarding the hydraulic conductivity of fractures, even sand placement may not outperform the wedge-shape-like sand distribution in the fracture. In our research before (Yue et al., 2020), we utilized a mixture model to study the sand placement in crack networks and evaluate the impacts of uneven sand placement on the productivity of an MHFW. However, due to the limitation of computational capacity, the scale of this fracture network is far from the real fracture networks, and the orthogonal fracture networks cannot fully represent the real situation for a fractured horizontal well. To sum up, current gasps in this research area call for further investigations on this topic. All these issues invite further investigation in this research area.

Second, during the development of unconventional oil resources within Chang-7 Unit, one of the most important issues that need to be addressed is the non-linear seepage flow in the reservoir matrix (Zhang et al., 2022b). Compared to the kinematic equation of Darcy's law, such a non-linear seepage flow has an extra threshold pressure gradient (TPG) term in its kinematic equation. In the past few decades, abundant experiments (Thomas et al., 1968; Prada and Civan, 1999) have validated the presence of such a term in the relation between flow rate and pressure gradient and formulated the corresponding kinematic equation. The appearance of the non-linear fluid flow can be explained by the occurrence of boundary layers in the tiny pores and possible interfacial activity among the grains and fluid (Wang et al., 2018). Fig. 1 explains the difference in the kinematic equation between the non-linear seepage flow and Darcy flow (Liu et al., 2022). The kinematic equation containing TPG is a non-linear piece-wise function as shown in the figure, which is different from the linear kinematic equation of Darcy flow. Regarding oil or gas formations with the TPG effect, the fluid flow would not happen unless its local pressure difference is larger than the value of TPG. If the local reservoir pressure gradient is equal to

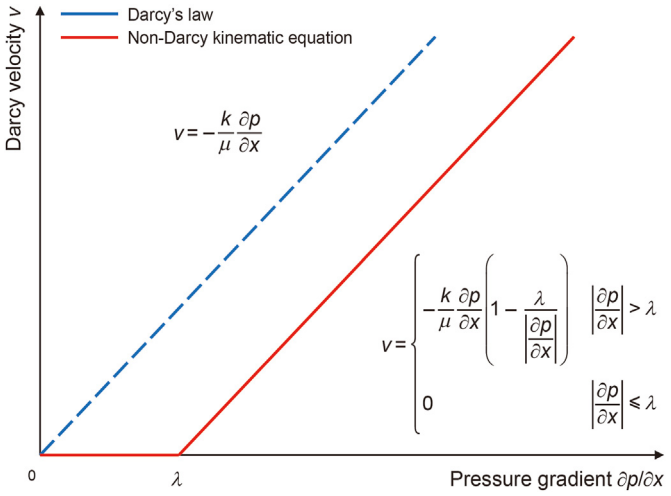

Fig. 1. Difference in the kinematic equation between Darcian and non-Darcian flow with TPG.

or smaller than the threshold value, no fluid flow in the reservoir matrix will be triggered. By contrast, when the local pressure gradient is higher than the threshold value, fluid can overcome the flow resistance and flow towards the wellbore. Therefore, an unconventional oil reservoir with TPG can be divided into two flow parts: (1) flow region: local pressure gradient is larger than the threshold value; (2) no-flow region: local pressure gradient is equal to or smaller than the threshold value. The boundary between the flow region and the no-flow region is the moving boundary, which can evolve over production time. It is distinctive from the classical Stefan moving boundary (Voller et al., 2004) since its moving speed is a function of the 2nd-order derivative of length. Fig. 2 shows the difference in pore pressure profile between conventional seepage flow and non-linear fluid flow with TPG, and an illustration of the TPG moving boundary.

In terms of non-linear fluid flow in the reservoirs with TPG, a great number of researchers presented fruitful analytical studies.

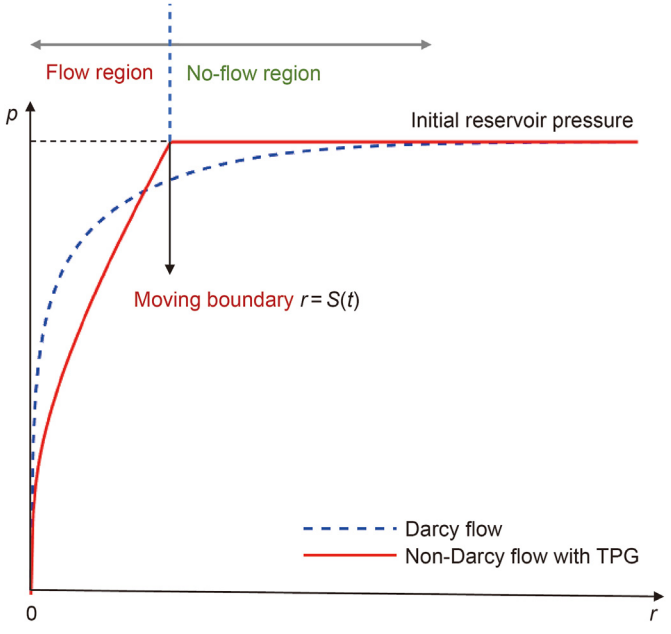

Fig. 2. Difference in pressure profile between Darcian and non-Darcian flow with TPG.

Zhu et al. (2011, 2022) studied how non-Darcy flow with TPG can affect the pore pressure distribution in the reservoir and also its impact on drainage areas in tight gas reservoirs. Liu and his co-workers (Liu et al., 2012; Liu, 2019) proposed a general exact analytical solution under one-dimensional and semispherical centripetal flow conditions in unconventional oil reservoirs with the low-velocity non-Darcian effect. However, for those unconventional reservoirs with ultra-low permeability, reservoir properties are usually heterogeneous which is difficult to be simply explained by analytical models. In terms of numerical models, some researchers conduct different kinds of studies but are still limited. The main gap is that the moving boundary induced by the non-linear flow cannot be described in their pseudo-linearized numerical approximation approaches. The reason behind this problem can be ascribed to the characteristic of the piece-wise formula in Fig. 1 and the accompanying high computational difficulty. To solve this problem, in our research before (Liu et al., 2019; Zhang et al., 2022a), we proposed a numerical workflow to effectively consider the threshold pressure gradient in the simulation model. In this workflow, we manually modified the gravity term in Darcy kinematic equation and thus incorporated the non-Darcy flow effect into the simulation process (Zhang et al., 2020). In this research, the numerical processing method of TPG still follows this way. Furthermore, we extend this method and thus the value of TPG in this research is dependent and varies with permeability rather than a constant value.

Although fruitful studies were presented in the past few years, there are still some critical gaps existing in this area. First, the fracture geometries in previous studies are relatively simple and cannot fully represent the real situation, especially for MFHWs. Then, for tight oil reservoirs in Chang-7 Member, non-linear fluid flow with TPG cannot be neglected, and such flow resistance may significantly impede the oil production from the reservoir and thus damage the production efficiency. The joint impact of proppant distribution and non-linear fluid flow should be studied to know how much overestimation in productivity would be yielded if we neglect their impacts. Those gaps in current studies require further research in this area.

The organization of this paper can be clarified as follows. First, the study area and the background information are illustrated in Section 2.1. Then, the core flooding experiments are carried out in Section 2.2 to figure out the relationship between TPG and permeability. Based on the reservoir background information and experimental results, all the mathematical models demanded by the integrated workflow are presented in Section 2.3. TPG is inserted into the calculation process by modifying the kinematic equation. After that, we establish the numerical models in Section 3.1 and conduct validations of individual models, respectively. Then, the impacts of the proppant distribution and TPG on fluid flow and reservoir development are studied in Sections 3.2 and 3.3. This research provides new insights into the development of the unconventional tight oil reservoir and meanwhile reveals the significance of proppant distribution and non-linear fluid flow in the production scenario design.

2. Methodology

2.1. Study area and geological background

In this study, the target area is located in Gansu Province, northwest of China. The study area has an area of 20,000 km^2 as shown in Fig. 3 and it contains abundant reserves of oil and gas. Currently, hundreds of wells are drilled here to exploit the unconventional oil reservoir in Chang-7 Unit. For the reservoirs

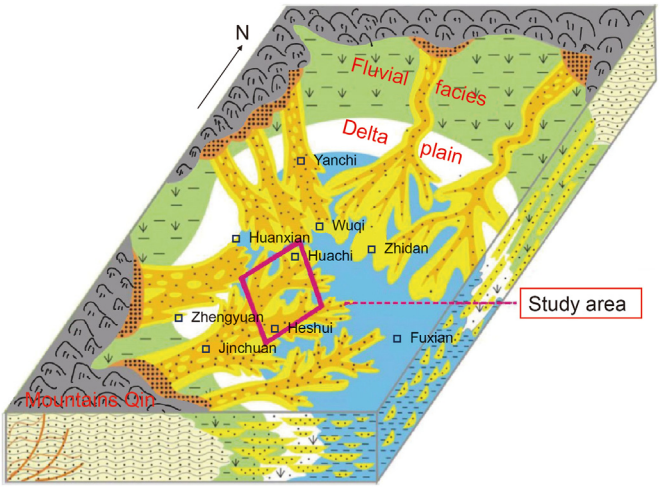

Fig. 3. Sedimentary facies and research area in Ordos Basin.

located in the study area, the porosity ranges from 4.0% to 12.9% and has an average value of 8.7%. The permeability in the study area is mainly between 0.01 and 1.55 mD and the mean value of 0.15 mD. The mean value of the radius of the throat in the reservoir matrix is 0.4215 μm.

2.2. Measurement of TPG in study area

One important characteristic for the fluid flow in the subsurface inside the study area is the threshold pressure gradient (TPG). Abundant research has revealed that, the presence of TPG can significantly impair well productivity and thus it is of vital importance to know the TPG value of the reservoir before any development. However, the value of TPG is highly correlated to the reservoir permeability and this correlation varies from area to area. Therefore, before we implement any formal analysis, an estimation equation of TPG for the study area should be derived from the core flooding experiments first.

In this research, the rock core samples were obtained from the Chang-7 tight oil reservoir in the study area. In order to derive a function between the value of TPG and permeability, core flooding experiments need to be carried out. The procedures of core flooding experiments can be referred to Tian et al. (2018). After the core flooding experiments, the TPG value can be inferred by simply reading the permeability value. Fig. 4(a) shows the results of the core flooding experiments. For a better understanding of the experimental results, here we use different colors to represent the data points from different cores. Besides, we also used fitting curves to summarize the trending of experimental data. For each fitting line, one can easily obtain the corresponding TPG value by simply reading the intercept in the x-axis. Fig. 4(b) shows the TPG value for each core as shown in scatted points and the relationship between TPG value and permeability can be calculated using a fitting curve.

According to the fitting curve in Fig. 4(b), the relationship between TPG and matrix permeability can be ruled out as shown in Eq. (1). The presented equation fits the data points perfectly since the correlative factor (R^2) is more than 0.99.

$$\lambda = 0.3267k^{-0.3537}, \tag{1}$$

where λ is the value TPG, MPa/m; k represents the permeability of porous media, mD.

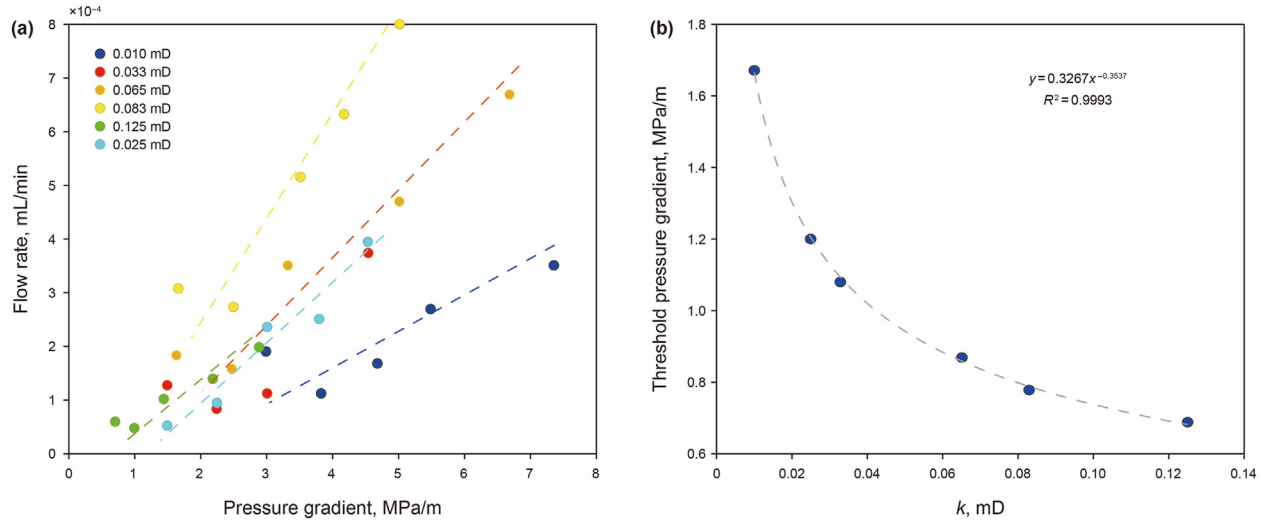

Fig. 4. Experimental results for the relationship between the pressure gradient and flow rate (**a**) and the relationship between TPG value and permeability (**b**).

2.3. Mathematical models

Since this study provides an integrated workflow to investigate the effect of (1) sand placement in fractures, and (2) non-linear fluid flow in reservoir matrix on horizontal well productivity, several mathematical models in this workflow should be clarified, respectively.

2.3.1. Proppant transport in induced fractures

During the reservoir stimulation, sands are injected into the induced cracks to prevent full closure of fractures and meanwhile provide high fracture conductivities. In most cases, those proppant particles are carried by proppant-laden fluid. Therefore, regarding the simulation of sand placement in hydraulic fractures, a solid phase, i.e., proppant, and a fluid phase, i.e., the proppant-laden fluid should be considered. Here, we utilized a solid–fluid mixture model to study the sand placement behavior inside cracks. This method has a great advantage in computational efficiency since it only solves one set of Navier-Stokes (N–S) equations. To accurately adopt the proposed mixture model, sever assumptions should be made including: (1) we neglect the variance in the density of proppants and fluid; (2) we assume that the proppant particles move in the fracture in a terminal speed.

The momentum balance equation for the mixture can be described as follows (Rao et al., 2002):

$$\rho_m \frac{\partial \boldsymbol{u}}{\partial t} + \rho_m (u_1 \cdot \nabla) u_1 = -\nabla p_1 - \nabla \cdot \left[\rho c_s (1 - c_s) u_{slip} \cdot u_{slip} \right] + \nabla \cdot \left[\eta \left(\nabla u_1 + \nabla u_1^T \right) \right] + \rho_m g, \quad (2)$$

where $\boldsymbol{u}$ is the mass-averaged velocity of the mixture; u_1 represents the average speed of the mixture; u_{slip} is the velocity difference between the proppant and laden fluid, m/s; c_s represents the mass fraction of proppant particles, dimensionless; η is the dynamic viscosity of the solid–fluid system, mPa·s; g is the gravity acceleration, m/s^2; ρ is the density of oil, kg/m^3; ρ_m is the density of the solid–fluid mixture density, kg/m^3, which can be described as:

$$\rho_m = (1 - \varphi_s)\rho_f + \varphi_s \rho_s, \quad (3)$$

where ρ_f is the density of the fluid phase, kg/m^3; ρ_s represents the density of the proppant back, kg/m^3; and φ_s is the volume fraction of sand (solid phase), kg/m^3.

We can calculate the viscosity η of the solid–fluid system as (Krieger and Dougherty, 1959):

$$\eta = \eta_f \left(1 - \frac{\varphi_s}{\varphi_{max}} \right)^{-2.5\varphi_{max}}, \quad (4)$$

where η_f denotes the fluid dynamic viscosity, mPa·s; φ_{max} denotes the maximum volume fraction of sand (solid phase) in the solid–fluid mixture.

The continuity equation for the solid–fluid mixture is as follows (Rao et al., 2002):

$$\left(\rho_f - \rho_s \right) \left\{ \nabla \cdot \left[\varphi_s (1 - c_s) u_{slip} \right] \right\} + \varphi_f (\nabla u_1) = 0. \quad (5)$$

One can obtain the transport equation of the solid phase as:

$$\frac{\partial \varphi_s}{\partial t} + \nabla \cdot (\varphi_s u_s) = 0, \quad (6)$$

where u_s is the moving velocity of the proppant particles in m/s as:

$$u_s = u_1 + (1 - c_s) u_{slip}. \quad (7)$$

Incorporating Eq. (7) into Eq. (6), we can get:

$$\frac{\partial \varphi_s}{\partial t} + \nabla \cdot \left[\varphi_s u_1 + \varphi_s (1 - c_s) u_{slip} \right] = 0. \quad (8)$$

Based on the equations above, we can simulate the proppant placement process during hydraulic fracturing using COMSOL Multiphysics.

2.3.2. Fracture conductivity estimation

After the proppants are placed, the propped fracture will gradually be closed due to the existence of *in-situ* stress. The fracture width and conductivity after the fracture closure are mainly determined by the proppant distribution. Based on the Carman-Kozeny equation (Carman, 1956) and Hertzian contact (Hertz, 1881), we constructed an analytical model for the estimation of hydraulic conductivity for cracks in our previous study (Zhu et al., 2019), which considered the proppant volume concentration, closure stress, proppant size, proppant material, and proppant embedment. Using this model, we convert the obtained proppant distribution to the fracture conductivity we need in the reservoir simulations.

We can calculate the propped fracture aperture as follows :

$$d_f = \frac{2\sqrt{6}}{3} r \times \left(\frac{2\sqrt{3}(1 - B_t) C r^2}{m_o} - 1 \right) + 2r - 2h_1, \tag{9}$$

where d_f denotes the crack aperture after closure, m; r is the radius of a proppant particle, m; C is the proppant concentration, kg/m^2; m_o is the mass of a single sand particle, kg; B_t is the breakage rate, dimensionless; h_1 is the embedment distance, m, which can be calculated as follows

$$h_1 = \sqrt[3]{\frac{9}{16r} \left(\frac{1 - \upsilon^2}{E} + \frac{1 - \upsilon_1^2}{E_1} \right)^2 F^2}, \tag{10}$$

where E and E_1 are Young's modulus of a single sand particle and the reservoir rock, Pa; υ and υ_1 are the Poisson's ratio of single sand particles and the reservoir rock; F denotes the force loaded to induvial proppant particle, N, which can be calculated as follows

$$F = p_c \times 2\sqrt{3} r^2, \tag{11}$$

where p_c is the closure stress, Pa.

Then we can obtain the permeability of the propped crack as:

$$k_f = \frac{\left(\frac{W_f - \frac{4}{3} n_o \pi r^3}{W_f} \right) \left(\left(\frac{2}{\sqrt{3}} - 1 \right) r \right)^2}{8\tau^2}, \tag{12}$$

where k_f is the permeability of the propped fracture, 10^{-3} μm^2; n_o is the proppant layers number in fracture; τ represents the tortuosity.

After we obtain the hydraulic conductivities for the propped fractures, we can incorporate those values into the reservoir simulation models and further evaluate the corresponding well performance. Besides, for the unpropped fractures (natural fractures if any), we can apply the cubic law to evaluate their fracture conductivities.

2.3.3. Seepage flow in cracks

Regarding the seepage flow inside the fracture system, in this paper we used a prevalent simulation for fracture flow, i.e., discrete fracture model (DFM) (Karimi-Fard et al., 2004). In DFM, the kinematic equation for seepage flow inside the crack is:

$$u_f = -\frac{k_f}{\mu} \nabla_T p_f, \tag{13}$$

where u_f represents the seepage speed in the crack direction, m/s; $\nabla_T p_f$ is the pore pressure gradient along the crack direction, Pa/m; μ is the fluid viscosity, Pa·s.

The continuity formula for seepage flow in hydraulic fractures is as follows:

$$\nabla_T \cdot \left(d_f \rho u_f \right) + d_f \frac{\partial}{\partial t} \left(\phi_f \rho \right) = 0, \tag{14}$$

where ρ represents the oil density, kg/m^3; ϕ_f represents the porosity of the proppant pack.

2.3.4. Seepage flow in reservoir matrix with TPG

Regarding the seepage flow in the reservoir matrix, we should consider the impact of TPG on fluid seepage (Prada and Civan, 1999). Therefore, the non-linear characteristic should be incorporated into the mathematical model by simply introducing an extra TPG term. The extended Darcy's law considering the TPG effect horizontal flow is (Liu et al., 2019):

$$\begin{cases} u_{m,\beta} = -\frac{k_{m,\beta}}{\mu} \frac{\partial p_m}{\partial \beta} \left(1 - \frac{\lambda_\beta}{\left| \frac{\partial p_m}{\partial \beta} \right|} \right), & \left| \frac{\partial p_m}{\partial \beta} \right| > \lambda_\beta \\ u_{m,\beta} = 0, & \left| \frac{\partial p_m}{\partial \beta} \right| \le \lambda_\beta \end{cases}, \tag{15}$$

where β can represent the different coordination direction, i.e., x and y; $k_{m,\beta}$ is the reservoir permeability, 10^{-3} μm^2; p_m represents the pore pressure, Pa.

The governing equation for seepage flow in the matrix is:

$$\nabla \cdot (\rho u_m) + \frac{\partial (\phi_m \rho)}{\partial t} = 0, \tag{16}$$

where u_m is the fluid velocity vector in the matrix; ϕ_m is the porosity of the matrix.

On the basis of the mathematical models presented before, one can seamlessly simulate the proppant injection, fracture closure and reservoir development respectively as shown in the flow chart of Fig. 5.

3. Results and discussion

3.1. Model description

According to the background information and methodology presented in the last section, an integrated workflow is established, and this workflow mainly consists of two simulation models. The first model is for the simulation of sand transport inside the cracks and the second model is for the reservoir simulation with TPG.

Fig. 6 shows the geometry model with the fracture paths in the reservoir in a 2-D map view. In this model, an MFHW is drilled, and the radius of both wellbores is 0.1 m. It is assumed that, for this horizontal well, 7 times of fracturing treatments are implemented so we have 7 stages of fractures along the wellbore direction. This initial fracture geometry is from previous simulation results of fracture propagation.

First, we need to establish the numerical model for the simulation of proppant transport in fractures. Since fractures usually have extremely high aspect ratios (fracture height: fracture width), simulation of particle flow inside the reservoir is not easy to converge and demands a higher quality of mesh generation. In this model, unstructured tetrahedron elements are used for meshing due to their high flexibility to deal with complex geometries. The diagram of generated mesh is shown in Fig. 7(a). Fig. 7(b) is a magnified diagram of mesh generation. In this model, we presume that we implement the fracturing job from stage #1 to stage # 7 in Fig. 7(a). Therefore, in the simulation model, proppants will be injected into the fractures stage by stage, from stage #1 to stage #7.

As we mentioned before, the simulation of proppant transport is difficult to converge due to the nature of the fracture geometry and needs further attention to model accuracy even if we have a converge. Therefore, before we implement any formal analysis, it is necessary to validate our numerical model. Here, we validate our model by simply checking the sand placement between the simulation results and experimental results. In the past few years, researchers have performed extensive physical experiments on sand placement in narrow spaces (cracks). Here, we choose the experimental results from Boronin and Osiptsov (2014) for comparison (Yue et al., 2020). Parameters in their experiments are shown in Table 1.

Fig. 8 shows the comparison of the shape of a sand dune. The similar sand slope curve and proppant distribution from the

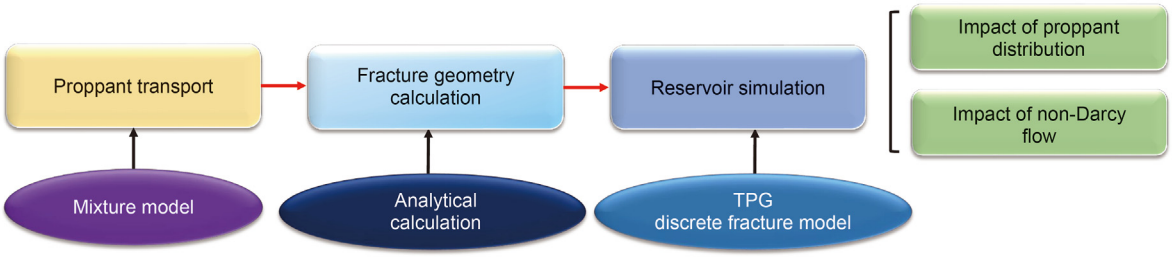

Fig. 5. Illustration of the presented integrated workflow.

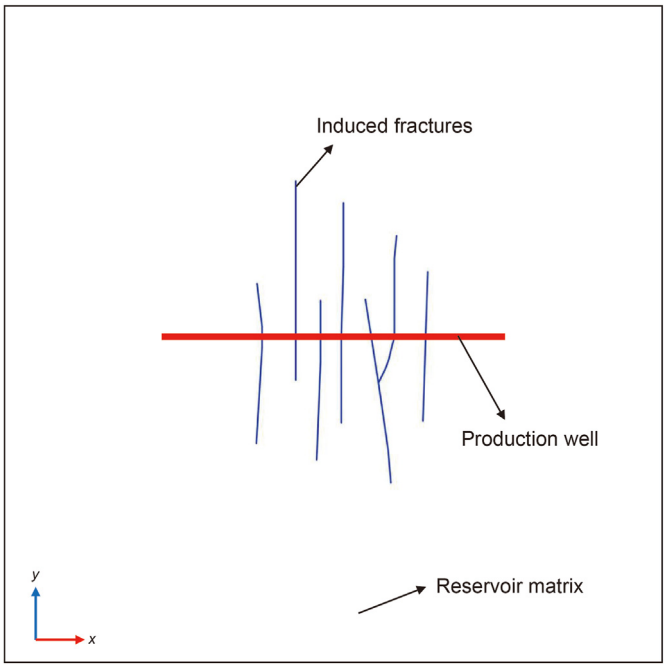

Fig. 6. Geometry model of geothermal formation with MFHWs in 2-D map view.

comparison indicate that there is relatively high accuracy for the numerical model.

Second, after we establish the simulation model for proppant transport, we need to incorporate its results into the reservoir simulation model. Since we consider the threshold pressure gradient in our reservoir simulation model, further mesh refinement should be performed near the fracture and the wellbore. In this model, unstructured tetrahedron elements are used for meshing due to their high flexibility to deal with complex geometries like wellbores and fractures. Fig. 9 presents the mesh information according to the reservoir simulation model.

Table 1
Experimental parameters for model validation (Boronin and Osiptsov, 2014).

Parameter	Value
Slot dimensions, mm	1500 × 160 × 5
The volume fraction of solid phase at the inlet, %	2
Density of laden fluid, kg/m^3	1000
Density of sand, kg/m^3	2600
Velocity of injection, cm/s	9.63
Particle radius, mm	0.075

Furthermore, to avoid the potential numerical diffusion and instability caused by unreasonable mesh generation scenarios, we also conduct a grid independence test for the reservoir simulation model. The goal of this grid independence test is to determine the minimum grid element number to produce reliable numerical results. Here, we design 4 simulation scenarios dedicated to the grid-independent test as shown in Table 2.

To quantitatively evaluate the mesh quality for each scenario, here we compare the evolution of reservoir pressure over 1000 days of production at a reference point with the coordination of (−50, 100, 0). Fig. 10 presents the comparison of reservoir pressure at the reference point between different mesh generation conditions. We could know from the comparison that, as the mesh generation for the model gets coarser, a clear numerical diffusion can be observed. When Gird #4 is implemented for the mesh generation of the simulation model, i.e., 134,959 elements, the corresponding reservoir pressure at the reference point is obviously different from other mesh generation conditions. After that, as the total element number rises, the output pressure value at the reference point becomes closer to each other. We can hardly see

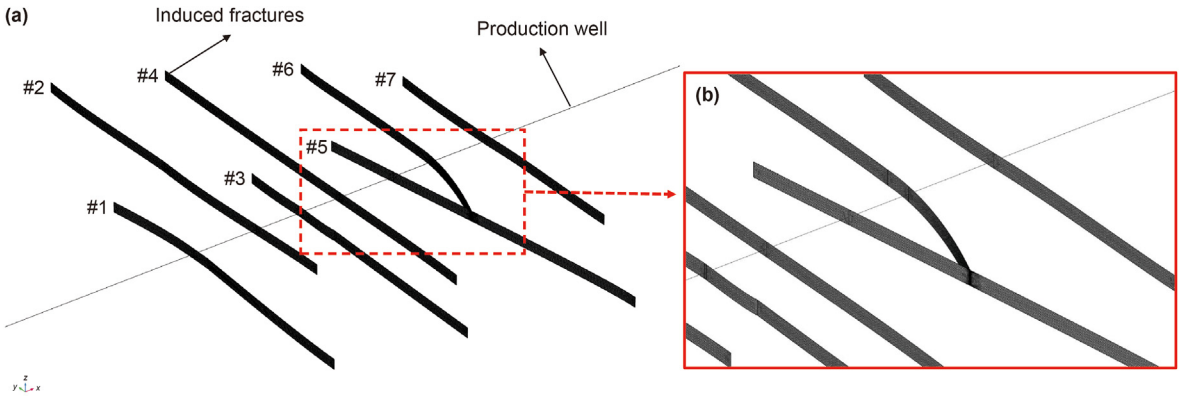

Fig. 7. Mesh information for the first simulation model.

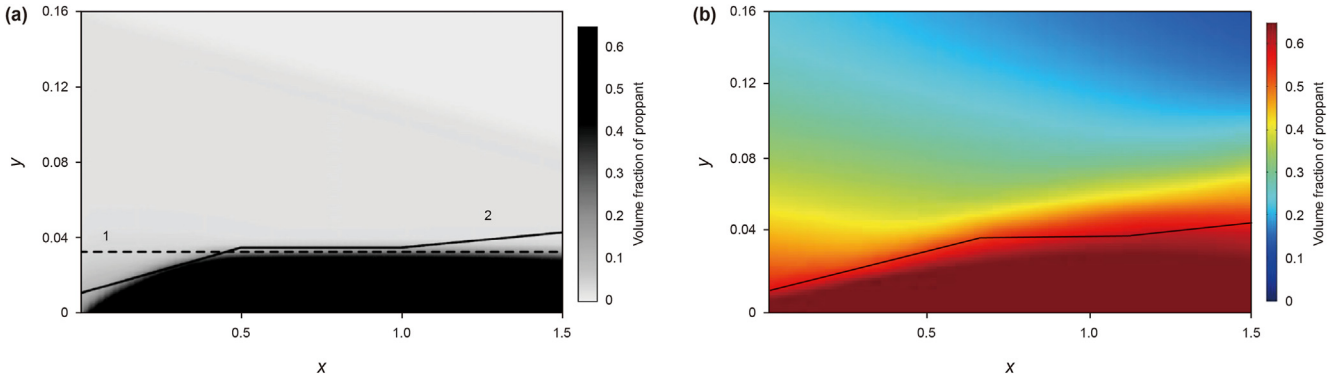

Fig. 8. The comparison of proppant distribution between experimental (**a**) and numerical (**b**) results (modified from Yue et al., 2020).

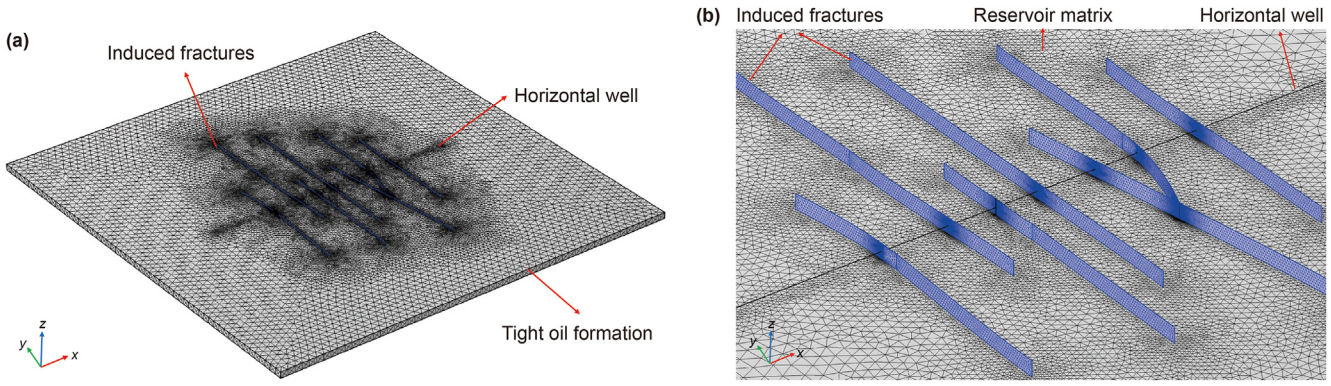

Fig. 9. Mesh information of the reservoir simulation model. (**a**) Mesh grids for the simulation model; (**b**) Magnified diagram of mesh grids for the simulation model.

Table 2
Different scenarios for grid independence test.

Scenario	Situation	Mesh category	Total element
Grid #1	Very dense	Unstructured tetrahedron element	978432
Grid #2	Dense	Unstructured tetrahedron element	523491
Grid #3	Medium	Unstructured tetrahedron element	279182
Grid #4	Coarse	Unstructured tetrahedron element	134959

any difference between cases Grid #1 and Grid #2. In other words, if we keep increasing the number of total grids, we may not receive further benefits from it. Therefore, in this paper, we choose Gird #2 with 523,491 elements for mesh generation of the simulation model, considering both the calculation cost and the model accuracy.

Before running a detailed numerical analysis, it is necessary to test and calibrate the parameters for the numerical solver to breed good stability, and accuracy of the model. Detailed parameter settings for the solver are listed in Table 3.

To make the numerical model can effectively and accurately reproduce the real situation, here we compare the daily oil rate calculated from the simulation model and the real oil rate from a horizontal well in an unconventional oil reservoir in the target area. Table 4 lists some basic parameters for the model validation.

Fig. 11 shows the numerical simulation results and the production data from the oilfield. The black scatter points in the figure represent the real daily oil data during the real production of a tight oil reservoir. The red line in the figure represents the calculated results from the presented numerical workflow. In general, the red line can closely fit the real production data and thus there is relatively high accuracy for the numerical model.

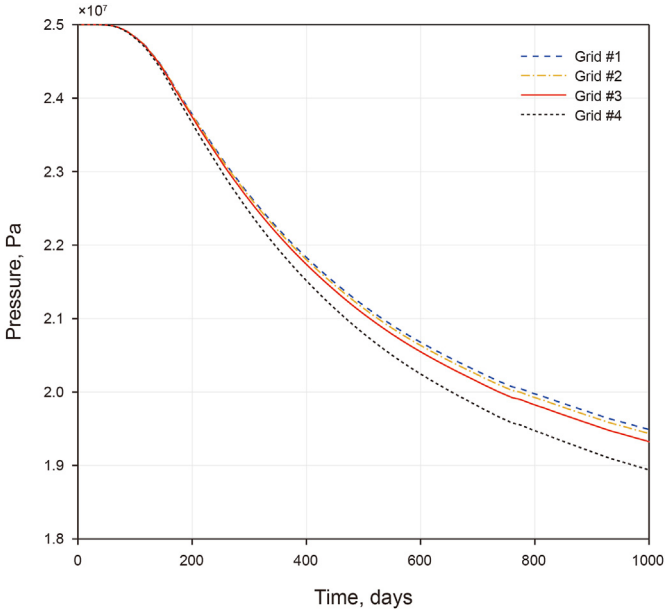

Fig. 10. Reservoir pore pressure at the reference point between different mesh generation scenarios.

Table 3
Parameters for the numerical solver.

Parameter	Value
Time-dependent solver	MUMPS
Time stepping method	Backward differentiation formulas (BDF)
Max order of BDF order	2
Min order for BDF	1
Tolerance during iterations	0.01
Initial size of time step, day	0.001
Max size of time step, day	50

Table 4
Parameters for model validation.

Parameter	Value
Intrinsic porosity of reservoir matrix, %	12
Intrinsic permeability of reservoir matrix, μm^2	0.1×10^{-3}
Formation thickness, m	15
Bottomhole pressure, Pa	0.5×10^7
Initial pore pressure, Pa	1.5×10^7
Oil density, kg/m^3	850
Oil viscosity, mPa·s	1.27

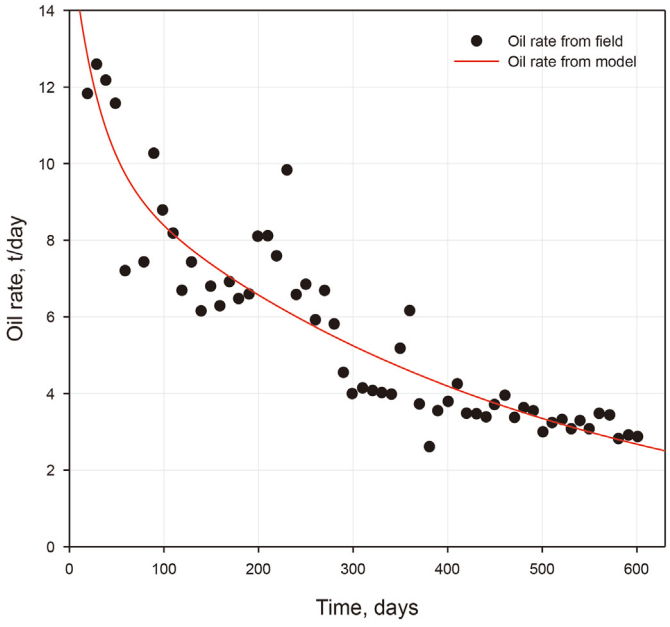

Fig. 11. Illustration of calculated oil rate and field data.

3.2. Impact of proppant placement on horizontal well productivity

In Section 3.1, we have designed the numerical workflow for simulation purposes. On this basis, numerical simulations are performed here to study the impact of proppant distribution on the productivity of MFHWs. As we mentioned before, the integrated workflow we presented in this study mainly consists of two parts of simulations. First, we need to simulate the proppant transport inside cracks. Parameters for this part of the simulations are listed in Table 5.

Fig. 12 indicates the sand distribution in the fracture system initiated from the horizontal production well. It could be seen from the figure that the proppant placement is apparently not as idealized as we expect. Significant uneven proppant distribution can be identified in the fracture systems: There are few proppants that can

Table 5
Parameters for the numerical model.

Parameter	Value
Fracture height, m	15
Fracture aperture during sand injection, cm	2
Density of sand, kg/m^3	2200
Velocity of mixture injection, m/s	0.45
Density of laden fluid, kg/m^3	1250
Diameter of proppant particle, μm	320
Volume fraction of solid phase in the mixture	0.2
Viscosity of fluid, mPa·s	5.1
Injection time for each stage, s	250
Total calculation time for seven stages, s	1750

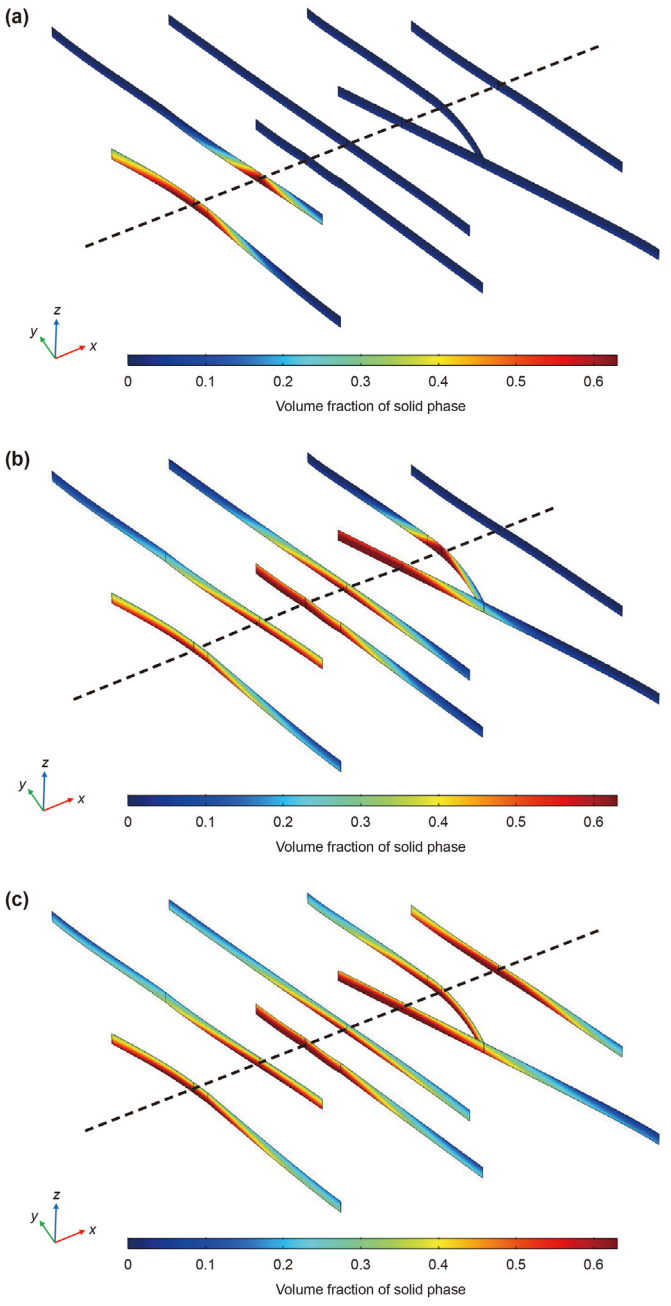

Fig. 12. Diagram of volume fraction of solid phase in induced fractures at 350 s (**a**), 1300 s (**b**), and 1750 s (**c**).

be delivered to the tip of cracks, while the sand concentration at the fracture root can reach its maximum value, i.e., 0.63.

After we have the distribution of solid phase volume fraction in the fracture system initiated from the horizontal well, we can get the fracture conductivity for the reservoir simulations. Parameters for this section are shown in Table 6.

Fig. 13 presents the distribution of the pore pressure profile after 200, 500, and 1000 days of production, respectively. It could be seen from the comparison that, as time marches on, the drainage area will continuously expand. However, most of the pressure drops in the reservoir concentrates near the fracture root. Regarding the fracture tip, the pressure drop is much smaller. The explanation of this characteristic of the pore pressure profile is that more proppants settle down in the fracture root and generate much higher fracture conductivity. By comparison, since few proppants can be placed near the fracture tip, this part of fracture are not very conductive.

In the past few decades, extensive reservoir simulations with hydraulic fractures presumed that fractures are fully propped and have infinite conductivity. The uneven proppant distribution was dismissed in those studies. However, due to the nature of proppant transport behavior, actually, there are few proppants that can really touch the fracture tip and provide effective hydraulic conductivity there. Therefore, given the highly unbalanced sand placement in the fracture system, the geometry and hydraulic conductivity of cracks at different locations after closure may also significantly vary. Therefore, during the reservoir simulation, different treatments or assumptions for the propped fracture can lead to distinguishing simulation results, including oil production. The results above in Fig. 13 illustrate the uneven sand placement and corresponding pressure distribution in the reservoir at different times. However, if we want to know the impact of proppant distribution on the development of a tight oil reservoir, we still need to compare the pore pressure distribution between simulation cases considering and not considering the uneven sand placement.

In this section, we utilized simulation models to quantitatively analyze the impacts of sand placement on reservoir development. The pore pressure profile in a 2-D plane view with unbalanced sand placement is as shown in Fig. 14. The pore pressure profile in a 2-D plane view with uniformed sand placement is as shown in Fig. 15. We can easily identify from the comparison between Figs. 14 and 15 that, sand placement has significant impacts on the reservoir drainage area. If the uneven proppant distribution in the fractures is considered, the sand concentration near fracture tips is quite limited. The corresponding drainage area is also limited according to Fig. 14(b). By contrast, when the idealized sand placement in the cracks system is considered, the corresponding hydraulic conductivity throughout the fracture network would be the same and thus the corresponding reservoir drainage area in Fig. 15(b) is much larger than those in Fig. 14(b). To sum up, the dismissal of uneven proppant distribution may overestimate the drainage area in the reservoir and thus affect the calculation accuracy of the well productivity.

Table 6
Parameters for the reservoir simulations.

Parameter	Value
Permeability of reservoir matrix, mD	0.2
Intrinsic porosity of reservoir matrix, %	10
Intrinsic porosity of the hydraulic fractures, %	15
Initial pore pressure, Pa	2.5×10^7
Bottomhole pressure (BHP), Pa	1.5×10^7
Initial oil density, kg/m^3	850
Oil viscosity, mPa·s	5

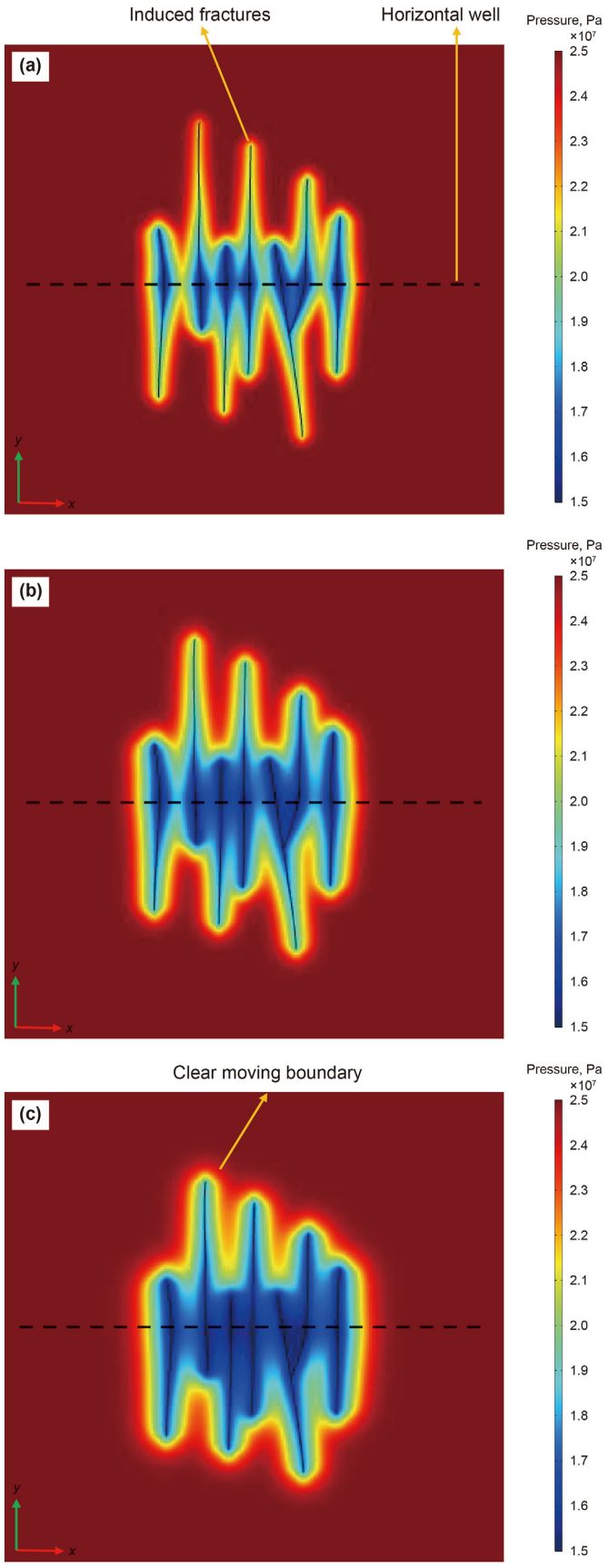

Fig. 13. Comparison of pore pressure profile in the tight oil reservoir according to different production times: (**a**) 200th day, (**b**) 500th day, (**c**) 1000th day.

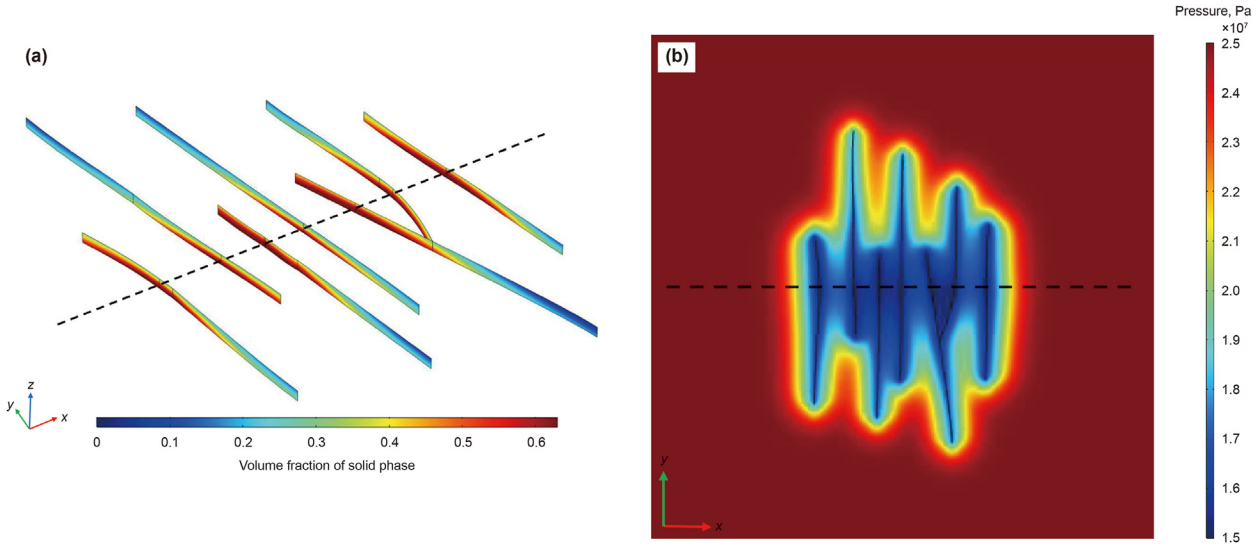

Fig. 14. Uneven proppant distribution (**a**) and corresponding reservoir pressure distribution (**b**).

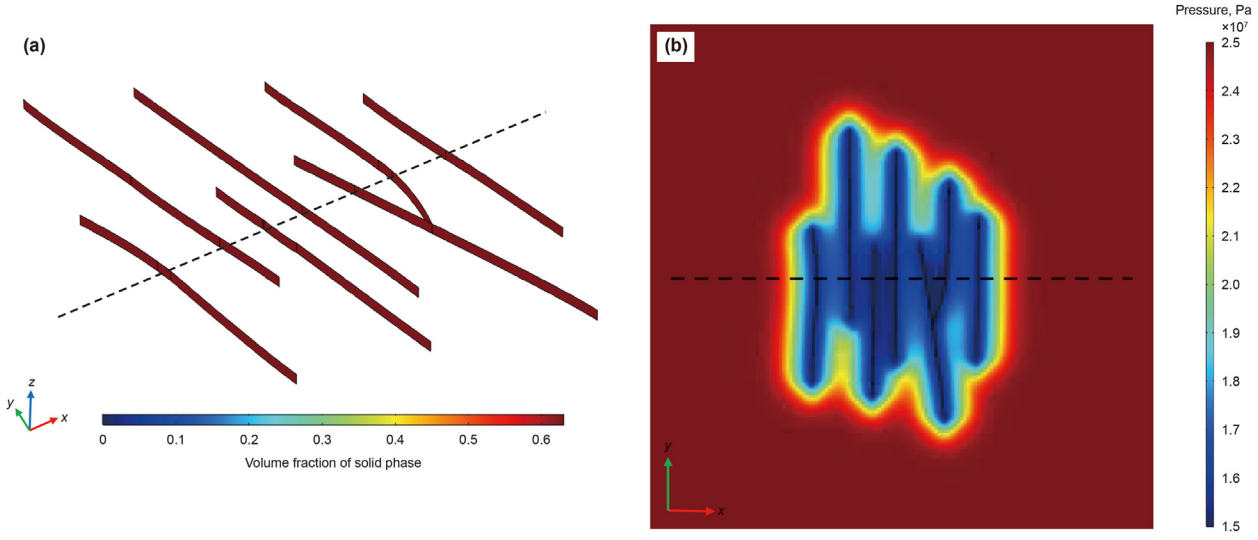

Fig. 15. Idealized proppant distribution (**a**) and corresponding reservoir pressure distribution (**b**).

Fig. 16(a) shows the comparison of daily oil rates according to the different simulation cases. We can see from the comparison that sand placement brings significant impacts on reservoir development. If we incorporate the uneven proppant distribution in the fractures into the model, the daily oil rate can reach 2.71 t/day after 1000 days of production. By contrast, when the idealized proppant distribution in the fractures is considered, the corresponding daily oil rate can reach 3.93 t/day, which is 44.98% higher than that in the simulation case with uneven proppant distribution. Fig. 16(b) shows the comparison of cumulative oil rates according to the different simulation cases. If we incorporate the uneven proppant distribution in the fractures into the model, the cumulative oil rate can reach 4552.8 t after 1000 days of production. By contrast, when idealized proppant distribution in fractures is considered, the corresponding cumulative oil rate can reach 5947.4 t, which is 30.63% higher than that in the simulation case with uneven proppant distribution. To sum up, under the model conditions, the neglect of uneven proppant distribution may overestimate the well productivity by 30.63%, which is considerable in the reservoir development process.

3.3. Impact of TPG on horizontal well performance

For the tight oil reservoir in the target area, operators found that the TPG has significant negative influences on well performance. Therefore, for a better understanding on how TPG would affect the production process, here two different simulation scenarios are designed as follows:

As we mentioned before, the moving boundary is an important characteristic for the exploitation of unconventional tight oil reservoirs with TPG. The occurrence of the moving boundary can be attributed to the piece-wise kinematic equation when TPG is considered in the mathematical model. Fig. 17 shows the comparison of pressure profiles between different simulation cases as designed in Table 7. From the comparison, we can see that, when we neglect the effect of TPG in the numerical simulation, we cannot observe any clear moving boundary and the pressure transition from the near-wellbore area to the deep reservoir area is continuous. By contrast, when the TPG is incorporated into the simulation model, we can identify a clear moving boundary. Besides, the corresponding drainage area in Scenario 2 is also much more limited than that in Scenario 1.

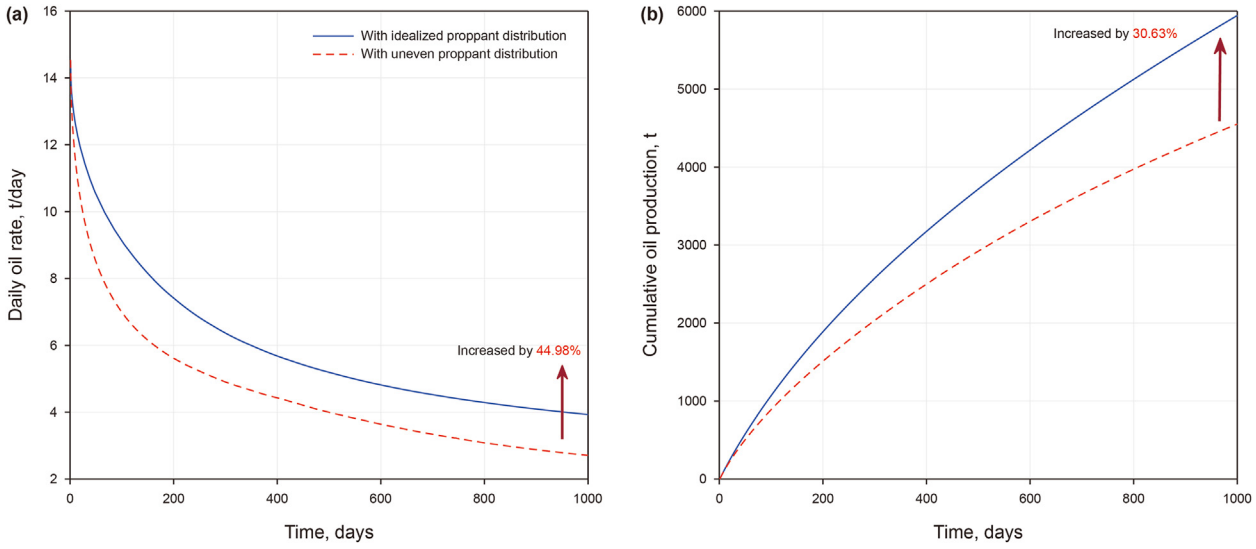

Fig. 16. Comparison of the daily (**a**) and cumulative (**b**) oil production over 1000 days according to different simulation cases.

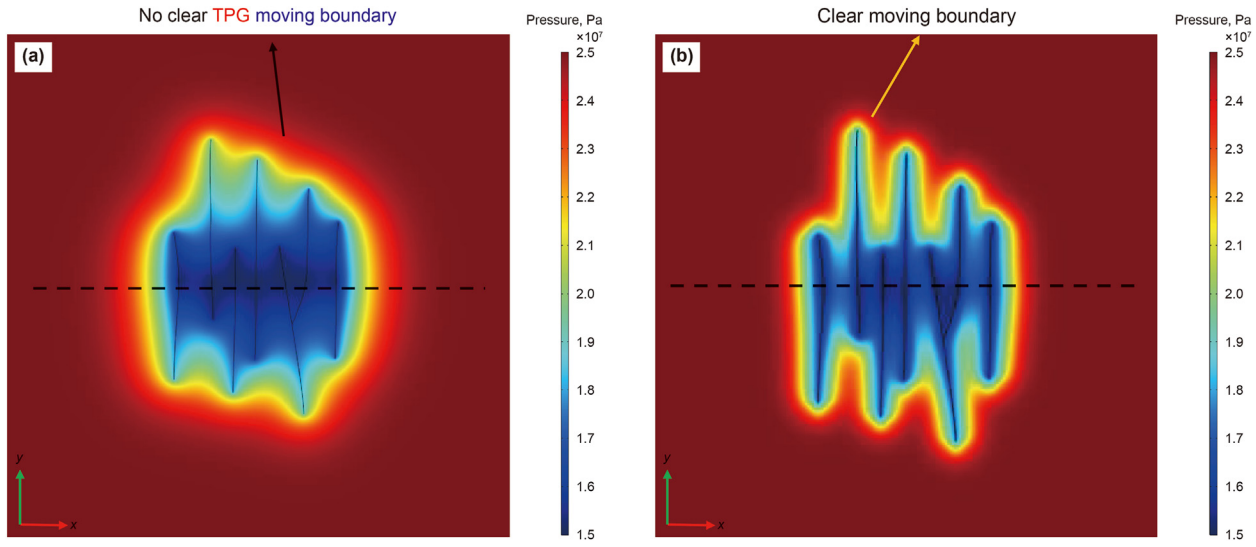

Fig. 17. Comparison of pressure profile in the tight oil reservoir at the 1000th day between Scenario 1 (without TPG) (**a**) and Scenario 2 (with TPG) (**b**).

Table 7
Simulation scenario design for comparison.

Simulation case	Matrix	Fractures
Scenario 1	Darcy's law	Proppant placement from Section 3.2
Scenario 2	Non-linear flow with TPG	Proppant placement from Section 3.2

Fig. 18 shows the comparison of the streamline distribution in the tight oil reservoir between different simulation cases after 1000 days of production. We can know from Fig. 18(a) that, when we neglect the negative impact of TPG during reservoir development, the streamlines are existent in all the reservoir areas of the model. The explanation for the large existent streamline is that Darcy fluid flow will be triggered as long as we create any pressure difference in the subsurface. By contrast, when the TPG is not incorporated into the model as shown in Fig. 18(b), we can see two different flow regions in the reservoir. These two regions can be divided by the TPG moving boundary. Inside the no-flow region, there is no streamline, i.e., there is no fluid flow in this area. Streamlines only exist in the flow region. The explanation for this distinguishing streamline distribution is that inside the no-flow region, the pressure gradient is zero so no fluid flow cannot be triggered and we can extract any oil from this area theoretically. It is worth mentioning that, the characteristic of a streamline profile is strictly consistent with Eq. (15).

To quantitatively evaluate the impact of TPG on well performance, Fig. 19 presents the comparison in cumulative oil production over the 1000 days of production between Scenario 1 (without TPG) and Scenario 2 (with TPG). We can easily identify from the

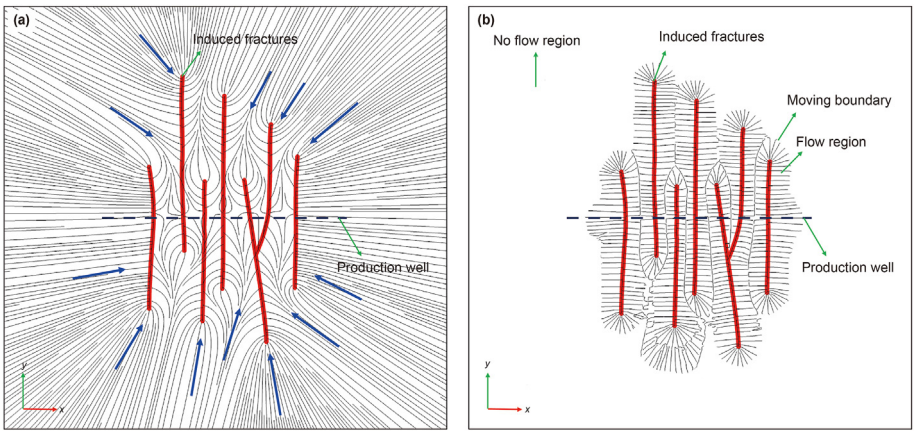

Fig. 18. Comparison of streamline distribution in the tight oil reservoir at the 1000th day between Scenario 1 (without TPG) (**a**) and Scenario 2 (with TPG) (**b**).

comparison that, the presence of TPG has significant impacts on horizontal well performance. When we neglect the negative impacts of TPG during the production process, the cumulative oil rate can reach only 4552.8 t after 1000 days of production. By contrast, when the TPG in the reservoir matrix is not incorporated into the model, the corresponding cumulative oil rate can reach 7642.5 t, which is 77.82% higher than that in the simulation case with TPG. To sum up, under the model conditions, the neglect of the TPG effect may overestimate the well productivity by nearly 80%, which may mislead the operators to make any inappropriate decisions for the field development.

4. Conclusions

In this research, we presented an integrated workflow to study the effects of (1) sand distribution in fractures and (2) non-linear flow in the reservoir matrix on the development of the reservoir. The geological information is derived from the unconventional oil reservoirs in Chang-7 Unit, northwest of China. Compared with our research before (Yue et al., 2020), here we extended this study into the development of multi-stage fractured horizontal wells (MFHWs) with large-scale complicated fracture geometry. According to the simulation results, some conclusions can be inferred as follows.

(1) Proppant distribution in a fracture system can significantly affect the performance of the fractured horizontal. When we assign an idealized proppant distribution in the fractures instead of the real proppant distribution, an overestimation of 44.98% in daily oil rate and 30.63% in cumulative oil production can be expected after 1000 days of development.
(2) TPG also significantly affects the oil production from the reservoir. When we simply apply the linear Darcy kinematic equation to the fluid flow in the reservoir matrix, the cumulative oil production will be 77% higher than that with non-linear fluid flow in the reservoir matrix after 1000 days of development.

In general, this research provides new insights into the development of unconventional oil reservoirs and meanwhile reveals the importance of proppant distribution and non-linear fluid flow in the production scenario design.

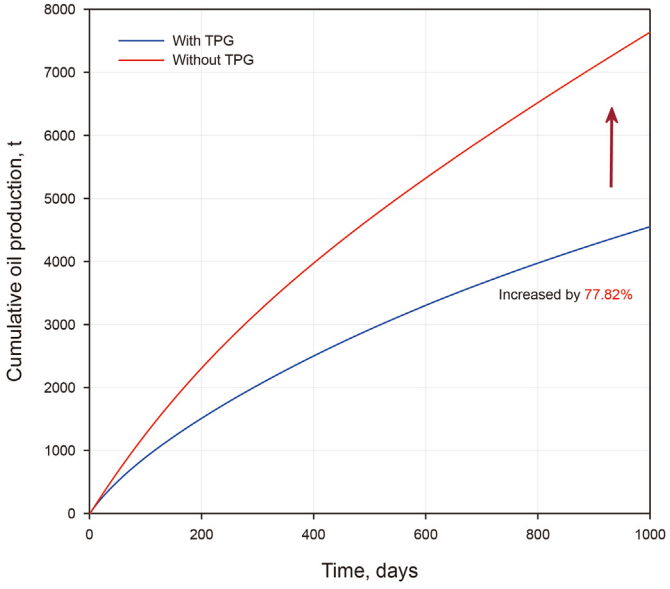

Fig. 19. Comparison of the cumulative oil rate between Scenario 1 (without TPG) and Scenario 2 (with TPG).

Declaration of competing interest

The authors declare that they have no known competing financial interests or personal relationships that could have appeared to influence the work reported in this paper.

Acknowledgments

The authors gratefully acknowledge the financial supports from the National Science Foundation of China under Grant 52274027 as well as the High-end Foreign Experts Recruitment Plan of the Ministry of Science and Technology China under Grant G2022105027L.

References

Boronin, S.A., Osiptsov, A.A., 2010. Two continua model of suspension flow in a hydraulic fracture. Dokl. Phys. 55 (4), 192–202. https://doi.org/10.1134/S0015462814020094.
Boronin, S.A., Osiptsov, A.A., 2014. Effects of particle migration on suspension flow in a hydraulic fracture. Fluid Dynam. 49 (2), 208–221. https://doi.org/10.1134/S1028335810040117.
Boronin, S.A., Osiptsov, A.A., Desroches, J., 2015. Displacement of yield-stress fluids in a fracture. Int. J. Multiphas. Flow 76, 4763. https://doi.org/10.1016/j.ijmultiphaseflow.2015.07.001.

Carman, P.C., 1956. Flow of Gases through Porous Media. Butterworths Scientific Publications, London.
Cleary, M., Fonseca Jr., A., 1992. Proppant convection and encapsulation in hydraulic fracturing: practical implications of computer and laboratory simulations. In: SPE Annual Technical Conference and Exhibition. https://doi.org/10.2118/24825-MS.
Dontsov, E., Peirce, A., 2014. Slurry flow, gravitational settling and a proppant transport model for hydraulic fractures. J. Fluid Mech. 760, 567–590. https://doi.org/10.1017/jfm.2014.606.
Dontsov, E., Peirce, A., 2015a. A Lagrangian approach to modelling proppant transport with tip screen-out in KGD hydraulic fractures. Rock Mech. Rock Eng. 48 (6), 2541–2550. https://doi.org/10.1007/s00603-015-0835-6.
Dontsov, E., Peirce, A., 2015b. Proppant transport in hydraulic fracturing: crack tip screen-out in KGD and P3D models. Int. J. Solid Struct. 63, 206–218. https://doi.org/10.1016/j.ijsolstr.2015.02.051.
Guo, Q., Wang, S., Chen, X., 2019. Assessment on tight oil resources in major basins in China. J. Asian Earth Sci. 178, 52–63. https://doi.org/10.1016/j.jseaes.2018.04.039.
Hertz, H., 1881. On the contact of elastic solids. Z. Reine Angew. Mathematik 92, 156–171.
Hu, X., Wu, K., Li, G., et al., 2018. Effect of proppant addition schedule on the proppant distribution in a straight fracture for slickwater treatment. J. Petro. Sci. Eng. 167, 110–119. https://doi.org/10.1016/j.petrol.2018.03.081.
Karimi-Fard, M., Durlofsky, L.J., Aziz, K., 2004. An efficient discrete-fracture model applicable for general-purpose reservoir simulators. SPE J. 9 (2), 227–236. https://doi.org/10.2118/88812-PA.
Krieger, I.M., Dougherty, T.J., 1959. A mechanism for non-Newtonian flow in suspensions of rigid spheres. Trans. Soc. Rheol. 3 (1), 137–152.
Liu, W., Yao, J., Wang, Y., 2012. Exact analytical solutions of moving boundary problems of one-dimensional flow in semi-infinite long porous media with threshold pressure gradient. Int. J. Heat Mass Transf 55, 6017–6022. https://doi.org/10.1016/j.ijheatmasstransfer.2012.06.012.
Liu, W., 2019. Analytical study on a moving boundary problem of semispherical centripetal seepage flow of Bingham fluid with threshold pressure gradient. Int. J. Non Lin. Mech. 113, 17–30. https://doi.org/10.1016/j.ijnonlinmec.2019.03.011.
Liu, W., Zhang, Q., Zhu, W., 2019. Numerical simulation of multi-stage fractured horizontal well in low-permeable oil reservoir with threshold pressure gradient with moving boundary. J. Petro. Sci Eng. 178, 1112–1127. https://doi.org/10.1016/j.petrol.2019.04.033.
Liu, W., Zhang, Q., Dong, Y., et al., 2022. Analytical and numerical studies on a moving boundary problem of non-Newtonian Bingham fluid flow in fractal porous media. Phys. Fluids 34 (2), 023101. https://doi.org/10.1063/5.0078654.
Osiptsov, A.A., Zilonova, E., Boronin, S., et al., 2016. Insights on overflushing strategies from a novel modeling approach to displacement of yield-stress fluids in a fracture. In: SPE Annual Technical Conference and Exhibition. https://doi.org/10.2118/181454-MS.
Osiptsov, A.A., 2017. Fluid mechanics of hydraulic fracturing: a review. J. Petr. Sci. Eng. 156, 513–535. https://doi.org/10.1016/j.petrol.2017.05.019.
Prada, A., Civan, F., 1999. Modification of Darcy's law for the threshold pressure gradient. J. Petro. Sci. Eng. 22, 237–240. https://doi.org/10.1016/S0920-4105(98)00083-7.
Rao, R., Mondy, L., Sun, A., et al., 2002. A numerical and experimental study of batch sedimentation and viscous resuspension. Int. J. Numer. Method. Fluid. 39 (6), 465–483. https://doi.org/10.1002/fld.246.
Suri, Y., Islam, S.Z., Hossain, M., 2020. Effect of fracture roughness on the hydrodynamics of proppant transport in hydraulic fractures. J. Nat. Gas Sci. Eng. 80, 103401. https://doi.org/10.1016/j.jngse.2020.103401.
Thomas, L., Katz, D., Tek, M., 1968. Threshold pressure phenomena in porous media. SPE J. 8 (2), 174–184. https://doi.org/10.2118/1816-PA.
Tian, W., Li, A., Ren, X., Josephine, Y., 2018. The threshold pressure gradient effect in the tight sandstone gas reservoirs with high water saturation. Fuel 226, 221–229. https://doi.org/10.1016/j.fuel.2018.03.192.
Voller, V.R., Swenson, J.B., Paola, C., 2004. An analytical solution for a Stefan problem with variable latent heat. Int. J. Heat Mass Tran. 47 (24), 5387–5390. https://doi.org/10.1016/j.ijheatmasstransfer.2004.07.007.
Wang, F., Liu, Z., Cai, J., et al., 2018. A fractal model for low-velocity non-Darcy flow in tight oil reservoirs considering boundary-layer effect. Fractals 26 (5), 1850077. https://doi.org/10.1142/S0218348X18500779.
Wang, J., Elsworth, D., 2018. Role of proppant distribution on the evolution of hydraulic fracture conductivity. J. Petro. Sci. Eng. 166, 249–262. https://doi.org/10.1016/j.petrol.2018.03.040.
Yao, S., Chang, C., Hai, K., et al., 2022. A review of experimental studies on the proppant settling in hydraulic fractures. J. Petrol. Sci. Eng. 208, 109211. https://doi.org/10.1016/j.petrol.2021.109211.
Yu, W., Zhang, T., Du, S., et al., 2015. Numerical study of the effect of uneven proppant distribution between multiple fractures on shale gas well performance. Fuel 142, 189–198. https://doi.org/10.1016/j.fuel.2014.10.074.
Yue, M., Zhang, Q., Zhu, W., et al., 2020. Effects of proppant distribution in fracture networks on horizontal well performance. J. Petrol. Sci. Eng. 187, 106816. https://doi.org/10.1016/j.petrol.2019.106816.
Zeng, B., Cheng, L., Hao, F., 2010. Experiment and mechanism analysis on threshold pressure gradient with different fluids. In: Nigeria Annual International Conference and Exhibition. https://doi.org/10.2118/140678-MS.
Zeng, B., Cheng, L., Li, C., 2011. Low velocity non-linear flow in ultra-low permeability reservoir. J. Petrol. Sci. Eng. 80 (1), 1–6. https://doi.org/10.1016/j.petrol.2011.10.006.
Zhang, Q., Dahi Taleghani, A., 2022. On the role of proppants and geomechanics on flowback behavior in complex fracture networks. J. Petrol. Sci. Eng. 216, 110835. https://doi.org/10.1016/j.petrol.2022.110835.
Zhang, Q., Zhu, W., Liu, W., et al., 2020. Numerical simulation of fractured vertical well in low-permeable oil reservoir with proppant distribution in hydraulic fracture. J. Petrol. Sci. Eng. 195, 107587. https://doi.org/10.1016/j.petrol.2020.107587.
Zhang, Q., Liu, W., Dahi Taleghani, A., 2022a. Numerical study on non-Newtonian Bingham fluid flow in development of heavy oil reservoirs using radio-frequency heating method. Energy 239, 122385.
Zhang, Q., Liu, W., Wei, J., et al., 2022b. Numerical simulation study on temporary well shut-in methods in the development of shale oil reservoirs. Energies 15 (23), 9161. https://doi.org/10.3390/en15239161.
Zhu, W., Song, H., Huang, X., et al., 2011. Pressure characteristics and effective deployment in a water-bearing tight gas reservoir with low-velocity non-Darcy flow. Energy Fuel. 25 (3), 1111–1117. https://doi.org/10.1021/ef1014633.
Zhu, W., Liu, Q., Yue, M., et al., 2019. Calculation of fracture conductivity considering proppant influence and simulation of proppant transport in fracture. Chem. Eng. Oil Gas 48 (2), 75. https://doi.org/10.3969/j.issn.1007-3426.2019.02.013 (In Chinese).
Zhu, W., Liu, Y., Shi, Y., et al., 2022. Effect of dynamic threshold pressure gradient on production performance in water-bearing tight gas reservoir. Adv. Geo-Energy Res. 6 (4), 286–295. https://doi.org/10.46690/ager.2022.04.03.